Extreme Mechanics Letters 63 (2023) 102067

Contents lists available at ScienceDirect

Extreme Mechanics Letters

journal homepage: www.elsevier.com/locate/eml

Excellent impact resistance of multilayer metallic glass films subjected to micro-ballistic impact by overcoming dynamic size effects

Yujie Cheng [a,c,1], Jinlei Dong [a,g,1], Yidi Shen [e,1], Fucheng Li [d], Qi An [e], Minqiang Jiang [c,f], Yanhui Liu [d], Chenguang Huang [c], William A. Goddard III [b], Xianqian Wu [a,c,*]

[a] Key Laboratory of Mechanics in Fluid Solid Coupling Systems, Institute of Mechanics, Chinese Academy of Sciences, Beijing 100190, China
[b] Materials and Process Simulation Center, California Institute of Technology, Pasadena, CA 91125, United States
[c] School of Engineering Science, University of Chinese Academy of Sciences, Beijing 100049, China
[d] Institute of Physics, Chinese Academy of Sciences, Beijing, 100190, China
[e] Department of Materials Science and Engineering, Iowa State University, Ames, IA 50011, United States
[f] State Key Laboratory of Nonlinear Mechanics, Institute of Mechanics, Chinese Academy of Sciences, 100190 Beijing, China
[g] Institute of Fluid Physics, CAEP, Mianyang 621999, China

ARTICLE INFO

Article history:
Received 4 May 2023
Received in revised form 4 July 2023
Accepted 14 August 2023
Available online 19 August 2023

Keywords:
Multilayered metallic glass
Impact resistance
Size effect
Micro-ballistic impact
Molecular dynamics simulation

ABSTRACT

Size effects are key issues that hinder the enhancement of impact resistance of films with increasing thickness. In this paper, we consider Ni_2Ta amorphous metallic alloy as a prototype thin film and demonstrate that the impact resistance of metallic glass (MG) nanofilms with surface oxidation subjected to micro-ballistic impact can be increased significantly by lamination of thin monolayers, overcoming significantly the size effects in the impact resistance of MG nanofilms. Shear band formation and delamination are the dominant energy dissipation mechanisms for multilayered films under impact. Our molecular dynamics (MD) simulations confirmed that the interfaces between thin layers as modified by surface oxidation play an important role in the impact resistance of the multilayered films. Surface oxidation of multilayered films increases significantly the impact resistance due to oxidation-induced curly structure and the increase of the interfacial strength, which contributes greatly to the energy dissipation during impact. However, excessive oxidation initiates defects near the surfaces of the monolayers to therefore reduce greatly impact resistance of the multilayered films. Our work suggests an effective pathway for fabricating high-performance multilayered MG films with extraordinary impact resistance by overcoming the size effects through the lamination of monolayers.

1. Introduction

Advanced materials with high-impact resistance are persistently required for both military and civilian applications such as protecting soldiers from high-speed bullets [1] and shielding spacecraft from debris [2]. In recent decades, metallic glasses (MGs) have attracted extensive attention and found a variety of engineering applications due to their unique mechanical and physical properties such as high strength, large elastic strain limit, and high fracture toughness [3–5].

Metallic glasses are also regarded as promising impact protective materials. Huang et al. [6] proposed a Whipple shield structure consisting of an amorphous alloy coating. Due to the relatively high density, low specific heat, and low melting temperature of the amorphous alloy, the unique Whipple shield structure showed much higher impact resistance under hypervelocity impact compared to the traditional Whipple shields. The study by Hofmann et al. [7] showed that using metallic glasses as intermediate layers for spacecraft leads to significantly increase in resistance of Whipple shields to hypervelocity impact of debris particles.

As the thickness is decreased to nanometers, amorphous alloy nanofilms subjected to micro-ballistic impact exhibit excellent impact resistance [8], which is equivalent to Kevlar fibers [9]. The shear bands, cracks, and bending of the impact-induced petals around the perforated hole are the main energy dissipation methods. Micro-ballistic impact experiments and molecular dynamics (MD) simulations by Cheng et al. [10] revealed the dynamic size effects of amorphous alloy films. The impact resistance of the amorphous nanofilms increased rapidly with decreasing thicknesses, indicating that higher impact resistance of MG films could be realized by fabricating with thinner thickness.

* Corresponding author at: Key Laboratory of Mechanics in Fluid Solid Coupling Systems, Institute of Mechanics, Chinese Academy of Sciences, Beijing 100190, China.
E-mail addresses: wag@caltech.edu (W.A. Goddard III), wuxianqian@imech.ac.cn (X. Wu).
[1] These authors contributed equally to this work.

https://doi.org/10.1016/j.eml.2023.102067
2352-4316/

To overcome the size effects of the impact resistance while fabricating relatively thick amorphous alloy films, a method that has attracted considerable interest in recent years is the layer-by-layer assembly of thin films with high impact resistance. This can improve the impact-protective performance of relatively thick films by optimizing the layering design and number of layers at the nanoscale [11–13]. The interactions between the layers could contribute to energy dissipation during impact. Dewapriya et al. [14] demonstrated through MD simulations that the specific energy absorption (SEA) of polymer/ceramic multilayered films could be improved remarkably by optimizing the individual layer thickness and their arrangement. However, there is not yet direct experimental proof that the excellent impact resistance of multilayered amorphous films can overcome the size effects by reducing the thickness of each monolayer.

To demonstrate this, we fabricated multilayered Ni_2Ta MG nanofilms through layer-by-layer (LBL) assembly. We then used Laser-Induced Projectile Impact Testing (LIPIT) to examine their impact resistance. Our experimental results showed that the SEAs of multilayered MG nanofilms were improved remarkably compared to the monolayer films with the same total thicknesses. The SEA of the multilayered MG nanofilm was almost at the same level as the individual thin monolayer, indicating that the size effect of the impact resistance of MG nanofilm was overcome significantly by the laminated fabrication. We also carried out MD simulations to investigate the impact response of the multilayered MG nanofilms, with results indicating that the interfaces between monolayers play an important role in the impact resistance of the multilayered films. After surface oxidation, the SEAs of the multilayered films increased significantly due to the oxidation-induced rough or curly structures and the increase of the interfacial strength, which contributed greatly to the energy dissipation during impact. However, excessive oxidation reduced greatly the impact resistance of the multilayered films, which we ascribed to the initiation of defects near the monolayer surfaces.

2. Methods

2.1. Micro-ballistic impact experiments

In this work, we extended our previous work on size effects of single MG nanofilm [10] to the ballistic impact response of multilayered MG nanofilms. Here we used Ni_2Ta MG as the model material due to its good glass-forming ability, ultrahigh strength, excellent impact resistance [8], and thermal stability [15]. The fabrication of the single Ni_2Ta MG nanofilms used the same method as Cheng et al. [10] As shown in Figure S1, the Ni_2Ta MG films oxidized inevitably during the preparation process. The thickness of the Ni_2Ta MG monolayers varied from 100 to 600 nm. We used the LBL assembly of three or six monolayer films with a thickness of 100 nm to obtain a multilayered film with a total thickness of 300 or 600 nm, respectively.

The experimental setup of the LIPIT platform was the same as described by Cheng et al. [10], which was originally developed by Lee et al. [16] and further improved by Veysset et al. [17] and Hassani-Gangaraj et al. [18] Before LIPIT, the aluminum microparticles were screened using molecular sieves with different screening sizes to ensure an almost uniform diameter of about 25 μm [10]. The launch speed of the micro-particle varied from 290 to 570 m/s by changing the laser pulse energy of the LIPIT platform. During the supersonic microprojectile impact, the multilayered Ni_2Ta MG films deformed under high strain rates ranging from 1.2×10^6 to 3.3×10^6 s^{-1} (Table S1). Due to the short penetration duration and the small ratio of the TEM grid length to the diameter of the micro-particle, we can neglect the influence of the boundary on the impact resistance performance of the films.

2.2. MD simulations

The MD simulations were performed with LAMMPS code [19], and the visualization of atomic structures was conducted with the aid of OVITO [20]. To investigate the Ni-Ta interaction of the multilayered Ni_2Ta MG films, we used the embedded atom method (EAM), which is regarded as one of the most effective force fields for metallic systems. The specific EAM parameters were derived from a recently developed EAM potential database of alloys, from which the alloy potentials can be determined by the normalized elemental potentials [21].

A typical melt-and-quench technique was used to fabricate Ni_2Ta MG monolayer nanofilms with a thickness varying from 1 to 3 nm. The length in the x, y direction is 31 nm. The cooling rate of the films during preparation was about 7×10^{11} K/s [22], which is sufficiently high to keep the metal atoms from rearranging back to the crystalline phase. Here, a monolayer film with a thickness of 1 nm was stacked twice and three times to obtain a multilayer film with a total thickness of about 2 and 3 nm, respectively. Since the experiments observe oxidation on the film surfaces, which changes both the mechanical behavior of the film and the interaction between layers, we included surface oxidation of the multilayered films. We used the Vienna Ab initio Simulation Package (VASP) [23,24] to generate the Density Functional Theory (DFT) data, specifically for the Ni-O and Ta-O interactions, which served as the basis for developing our Morse potential [25]. To accurately account for the exchange and correlation energy of electrons, we employed the Perdew–Burke–Ernzerhof (PBE) functional form of the generalized gradient approximation (GGA) [26,27]. Furthermore, we incorporated the D3 (Grimme–Becke–Johnson) corrections [28] to capture London dispersion interactions (Van der Waals attractions). The plane-wave projector augmented wave (PAW) method [27] was employed to produce pseudopotentials necessary for accurately describing the interaction between the core and valence electrons. For DFT simulations, we used an energy cutoff of 500 eV, which resulted in converged energies, forces, and geometries. Convergence was achieved with an energy threshold of 10^{-5} eV for terminating the electronic self-consistent field (SCF) calculations, along with a force criterion of 10^{-2} eV/Å. The K-point sampling was set at $4 \times 4 \times 1$ [29], with the z direction representing the vacuum direction. To minimize interactions between periodic images, a dipole correction [30] along the z direction was implemented. All calculations performed on the Ni-O system were spin-polarized. To calculate the binding energies, we firstly constructed a slab model with four layers for both Ni and Ta, of which the top 2 layers were allowed to relax and the bottom 2 layers were fixed. We also included a vacuum region of 15 Å along z direction to minimize the possible interactions between two periodic images. Then, we added one oxygen atom terminated on the surface and calculated the energy differences between the structures with different heights of O atom relative to the surface and the equilibrium point.

As shown in Fig. 1, the Morse potential has acceptable accuracy compared to density functional theory (DFT) results, indicating that it is appropriate for simulating the interaction of oxygen atoms with the Ni_2Ta MG nanofilms. In the meanwhile, we adjusted the area density of oxygen atoms ranging from 0.26 per nm^2 to 2.08 per nm^2 on each surface, to explore the influence of oxygen content on the impact resistance of the laminated films. The oxidized monolayer contracted and curled (Figure S2, see Supplementary Material for details), leading to the increase of thickness during the preparation process. For monolayers with a thickness of 1 nm, the final thickness after oxidation is ~1.5 nm.

Our experimental observations indicated that the deformation and fracture of the Al micro-bullets were negligible in the present

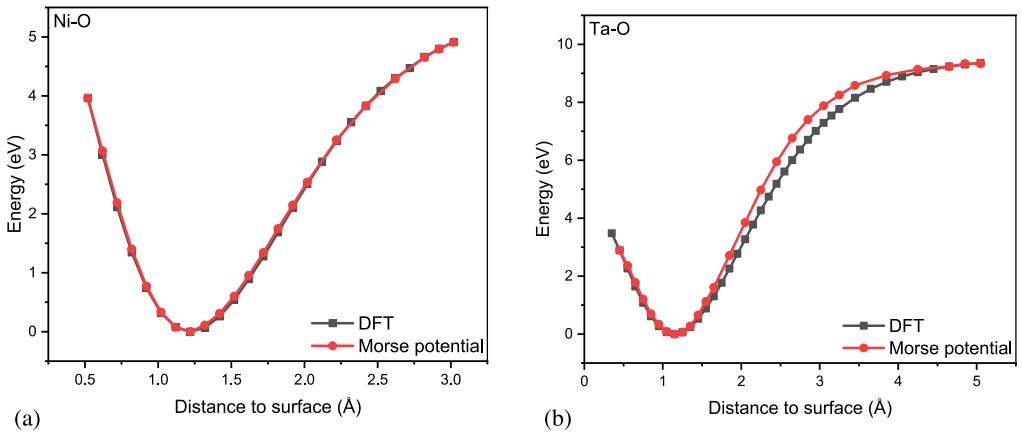

Fig. 1. Comparison of the DFT binding energy for (a) Ni-O and (b) Ta-O with our Morse potential.

impact velocity range. Therefore, we neglected the contribution of deformation and fracture of the Al micro-bullets to energy dissipation during the impact. Thus, aluminum projectile was constrained to retain its spherical rigid body shape modeled in the impact simulations. We adopted the Lennard-Jones (LJ) potential (6–12) to describe the interaction between the rigid Al ball and the Ni_2Ta MG multilayers. All potential parameters are summarized in Tables S2 and S3 (see Supplementary Material). We employed the velocity-Verlet time-step method with a 1 fs timestep for the metallic system in all simulations [31–33].

The impact model for MD simulations was the same as described by Cheng et al. [10]. The length of the oxidation film decreased from 31 nm to about 24 nm due to the curling and shrinkage of the film during the release of residual stress. The lengths of the films were more than (or equal to) four times the diameter of the projectile (6 nm) to minimize boundary effects [34]. If the impact velocity of the projectile was too high, a large number of high-speed fragments occurred in the front monolayer, resulting in the early failure of the bottom monolayers of the multilayered film [10]. In this case, it was useless to stack the Ni_2Ta MG nanofilms due to the premature failure of the top film. Hence, a series of impact tests were conducted with impact velocities ranging from 0.7 to 2 km/s to avoid high-speed fragments. However, the aluminum projectile could not fully penetrate the thin film (1–5 nm) at such low impact velocity. Therefore, we increased the molar mass of the bullet by a hundred times to obtain a heavier bullet with the same diameter, so that it had adequate penetration energy at relatively low impact velocities. This was different from experimental conditions, which might change the SEA of the multilayered films. Nevertheless, the MD simulations reveal the size effects and the energy dissipation mechanisms of the multilayered films under impact.

3. Results and discussion

3.1. Experimental results

In LIPIT experiments, the SEA E_p^*, which is defined as the scaled ballistic penetration energy by the mass of projected film volume, is employed to characterize the impact resistance of the nanofilm. Since the energy dissipation due to air drag during the impact process is much lower than the corresponding kinetic energy loss (see Supplementary Material), the ballistic penetration energy is approximately equal to the kinetic energy loss of the micro-bullet during penetration. The E_p^* of the Ni_2Ta MG monolayer and multilayer nanofilms with respect to the impact velocity were measured as shown in Fig. 2(a). The E_p^* increases significantly with increasing the impact velocity and with decreasing the thickness of the nanofilm, which is consistent with previous results [10]. To more visually illustrate the effect of thickness on the specific energy absorption of multilayered films, the SEAs of monolayered and multilayered Ni_2Ta MG nanofilms with respect to areal density are shown in Fig. 2(c). The SEA of the multilayered nanofilm with a total thickness of 300 nm (stacked by three 100-nm-thick monolayers) or 600 nm (stacked by six 100-nm-thick monolayers) is much higher than that of the monolayered film with the same total thickness. Intriguingly, the SEAs of the 3-layer and 6-layer multilayered Ni_2Ta MG films are almost the same as that of the 100-nm-thick monolayer films, indicating that the size effect of the Ni_2Ta MG films is overcome significantly, which provides a useful method for improving the impact resistance by stacking monolayer films. However, we can see that the SEA of the 6-layer film is slightly lower than the 3-layer film for the same impact velocity, showing the size effect of amorphous metallic films, as observed by Cheng et al. [10] remains for the multilayered films. As shown in Fig. 2(a), when the impact velocity is below a critical value of ~430 m/s for the 3-layer and 6-layer nanofilms, the SEAs of the laminated films can even exceed slightly that of the monolayered film, which we attribute to the interaction between layers at relatively low impact velocity. However, when the impact velocity is higher than the critical value of ~430 m/s, the SEAs of the multilayered films are slightly lower than that of the monolayer film due to the size effects [10].

The post-penetration SEM images of the damage zone of the multilayered Ni_2Ta MG nanofilms (6-layer, 600 nm) at different velocities are shown in Fig. 3(a) to further characterize the energy dissipation mechanisms. The perforation area increases with increasing impact velocity, indicating higher delocalized penetration energy. A typical penetration hole features a set of petals. The area beneath the bullet impact shows severe damage through folding, radial cracking, delamination, and loss of parts of the multilayer. During the impact process, the petaling cracks propagate away from the point of impact under the pressure of the penetrating projectile. The passage of the projectile through the target enlarges the circumference of the hole, extending the radial cracks. In addition, the radial cracks of the multilayered film increase with increasing impact velocity, indicating that the higher tangential stresses at 560 m/s were relaxed through additional radial cracks. In contrast to the simple petals at low impact velocity, extensively delaminated petals were observed at the perforation edge of the multilayered Ni_2Ta MG nanofilms under high impact velocity. We believe this deformation through delamination is also responsible for the high energy dissipation capacity. Fig. 3(b) shows the typical penetration morphology of the monolayered nanofilms at different impact velocities [8]. At the same thickness,

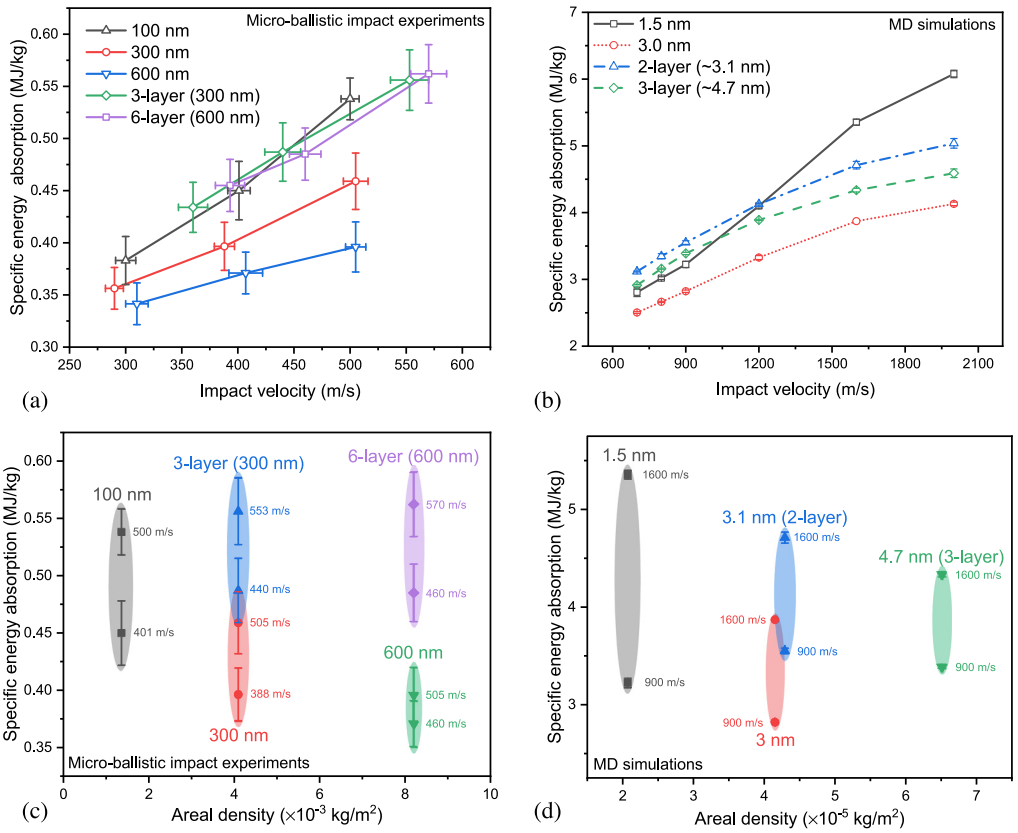

Fig. 2. Relationship between the specific energy absorption of the monolayered and multilayered Ni_2Ta MG nanofilms with various thicknesses and impact velocities obtained by (a) LIPIT experiments and (b) MD simulations. (c) and (d) show the measured and predicted specific energy absorption of the monolayered and multilayered Ni_2Ta MG nanofilms with various thicknesses with respect to areal density, respectively.

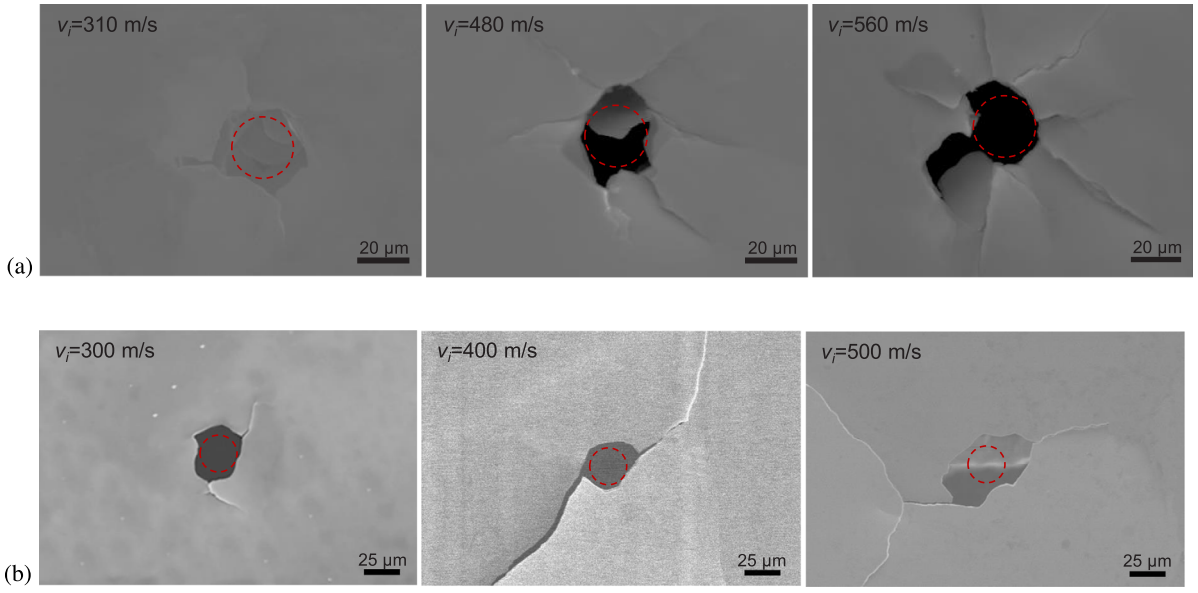

Fig. 3. Post-penetration SEM images of near-impact sites of the Ni_2Ta MG nanofilms at different impact velocities. (a) Multilayer films (6-layer for a total of 600 nm). (b) Single-layer films (600 nm). The red circles in the SEM images show the strike-face area.

the multilayered film shows obvious plasticity as demonstrated by the bending of petals. In sharp contrast, the destruction of the monolayered film shows typical brittle fracture of bulk MG materials [15]. MGs dissipate plastic energy mainly through localized shear bands [35], which include both nucleation and growth of the shear bands. Nucleation provides more plastic deformation by triggering the formation of new shear bands, whereas the growth process accelerates the failure of MGs, leading to eventual failure. Thus the deformation behavior of MGs is determined by the competition of energy dissipation between nucleation and propagation of shear bands [36]. As illustrated in Fig. 3, the failure morphology of the multilayered Ni_2Ta MG film shows shear band multiplication, which can remarkably improve the

plasticity of the Ni_2Ta film. In contrast, the failure of the monolayer with a thickness of 600 nm shows typical brittle fracture due to the limited plasticity provided by a single shear band propagation. Therefore, the impact resistance of the multilayered MG films is improved significantly due to the obvious plasticity, multiple crack initiation and propagation, and interfacial interactions. Based on the relatively high specific energy absorption, high melting temperature, and excellent thermal conductivity, the multilayered MG films could be used as advanced coatings to protect the surface integrity of materials especially under relatively high service temperature conditions such as turbine blade coatings and housing materials of smartphones.

3.2. Molecular dynamics simulations

We performed MD simulations aiming at providing an atomistic understanding of the dynamic response of the multilayered Ni_2Ta films under the micro-ballistic impact. Before the MD simulations, we examined whether non-oxidized multilayered films can explain the size effect of the impact resistance. Three 1-nm-thick non-oxidized monolayered films with different initial structures were stacked with an initial space of about 1 nm and then relaxed under the NVT ensemble to obtain energy-stable multilayered films. Due to the mutual attraction between the neighboring monolayers, the three monolayers eventually adhered together as a single thick film. Figure S3 (in Supplementary Material) shows the SEAs of the three-layered non-oxidized film with a total thickness of 3 nm, together with the 1-nm-thick and the 3-nm-thick monolayer non-oxidized films. The SEAs of the three-layered film with a total thickness of 3 nm and the 3-nm-thick monolayer are almost identical, which is not consistent with experimental observation, indicating that the interfaces modified by oxidation can significantly influence the impact resistance of the multilayered films.

Fig. 2(b). shows the MD-predicted SEAs of the multilayered surface oxidized Ni_2Ta MG nanofilms at various thicknesses and impact velocities. There are 82,420 Ni and Ta atoms and 1,000 O atoms in each 1.5-nm-thick monolayer film. We note that after oxidation the SEA of the Ni_2Ta MG monolayer increases significantly (Figure S4 in Supplementary Material). The peak force and its duration on the projectile for the oxidized monolayer are larger than the unoxidized film (Figure S5 in Supplementary Material), indicating that the curly structure of the oxidized film is beneficial to dissipate impact energy. For each thickness and velocity for the multilayered films, 3 independent penetration simulations were performed for statistical analysis by changing the random number for the initial atomic velocities. The MD simulation results in Fig. 2(d) show that the excellent protective performance of the multilayered films can be achieved by laminating the oxidized monolayers, which is consistent with the experimental results and some available data in the literature. Dewapriya et al. [37] also conducted MD simulations of ballistic impact tests on polyurea-aluminum multilayers to investigate the energy absorption and deformation mechanisms at the nanoscale. The results revealed that using multiple polyurea-aluminum layers does not have a significant advantage over bilayer structures. However, the SEAs of the multilayer structures are only slightly lower than that of the bilayer structures due to the presence of a large number of polymer–metal interfaces that could effectively contribute to energy dissipation under high-strain-rate impacts, indicating that the interface is important for the impact resistance of multilayered films.

For laminated films, there is a critical velocity below which the SEAs of the multilayered films are higher than that of the monolayers (1055 m/s for 3-layered nanofilms with a total thickness of ~4.7 nm), showing a reverse size dependence below the critical impact velocity. This indicates that the size effect of the impact resistance of the MG films depends on the impact velocity [10]. In addition, the critical velocity decreases with increasing the number of laminated films. However, above the critical impact velocities, the monolayers show higher SEAs, and the impact resistance of the multilayered films decreases with increasing the stacking number. This indicates that the deformation modes of the Ni_2Ta MG films depend on the impact velocities (Figure S6 for non-oxidized monolayer films in Supplementary Material and Fig. 4 for oxidized films). As shown in Fig. 4(a), above the critical impact velocities of 1600 m/s, plugging failure occurred for the multilayered films, which leads to premature failure of the material in the impacted area of the multilayered films and limits the delocalization of the impact energy dissipation during the impact process. As a result, the SEA of the multilayered film decreases with increasing total thickness. In contrast, the multilayered films exhibit larger conical deformation below the critical impact velocity, showing excellent delocalization energy dissipation capacity. Compared with the micro-ballistic impact experiments, the impact velocities in the MD simulations are a little higher and the thickness of the monolayers is much smaller, leading to the relatively higher SEAs and the severe plastic deformation observed in MD simulations. However, the MD simulation results still capture the phenomenon as observed in experiments and predict the dynamic behavior of the films at higher velocities.

The typical deformation behavior of the multilayered films during impact is shown in Fig. 5(a). At 3.6 ps, the projectile just hit the first layer of the multilayered Ni_2Ta MG film. As the projectile moves continuously, the three layers of the film experience conical deformation with the monolayers squeezing each other to consume the kinetic energy of the projectile during impact. Some obvious voids occur in the central impacted area of the film under tensile stress at 9.3 ps. The projectile penetrated completely the three-layered film at 18 ps. The dominant failure mechanism is local tearing around the projectile edge. However, no obvious hole formed in the MD simulation snapshots due to the rebound of the deformed region. The multilayered film exhibits localized thinning around the impact center. We believe that this thinning process results from film stretching during the impact process. Again, the severe plastic deformation of the multilayered films during impact in MD simulations results from the large plasticity of the 1.5-nm-thick monolayers due to the size effect, as discussed by Cheng et al. [10].

We also investigated the influence of oxygen content on the impact resistance of the multilayered Ni_2Ta MG films as shown in Fig. 5(b). For both the single-layered and the three-layered films, the SEA increases substantially after oxidation up to a coverage of 1.04 O per nm^2. However, it decreases when the O coverage further increases to 2.08 O per nm^2. To investigate the effects of oxidation, we calculated the average atomic potential energy of the three-layered films with different numbers of oxygen atoms as illustrated in Fig. 5(c). Here we partitioned evenly the three-layered films into seven regions along the thickness according to the atomic positions (whether the atoms are on the surface, interior, or at the layer-to-layer interface of the multilayered film) as shown in Figure S7. Regions consisting of surface atoms (the top and the bottom regions) were denoted as surface regions. The regions that include interfaces between two monolayers were denoted as interface regions, and the others were denoted as interior regions. For all MG films, the energy of the interface region is much higher than the interior regions. Most importantly, the high energy of the interface regions destabilizes the multilayered films, facilitating deformation in the interface regions compared to the interior regions. As the oxygen coverage increases, the difference between the energies of the interface regions and the interior regions increases quickly, indicating additional instability of the

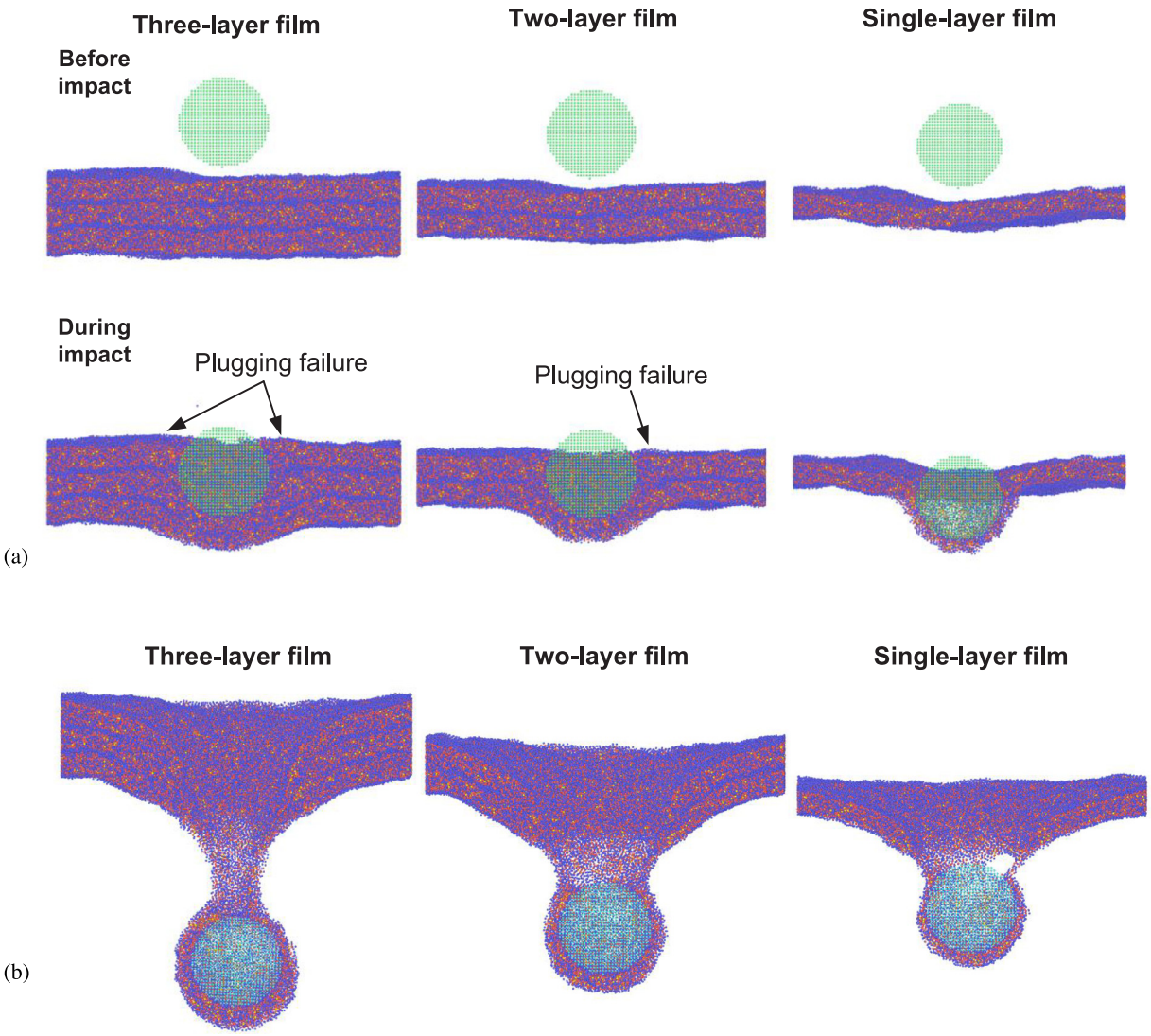

Fig. 4. Typical deformation behavior of the three-layered films, the two-layered films, and the single-layered films at (a) $v_i = 1600$ m/s and (b) $v_i = 900$ m/s from MD simulations.

interface regions during loading. This makes debonding of the interfaces between two neighboring monolayers during impact easier, which promotes the energy dissipation capacity of the multilayered films.

To understand the deterioration of the impact resistance of the multilayered films when the oxygen coverage is doubled to 2.08 O per nm^2, we stretched the two-layered films along the thickness direction using MD simulations to predict the interfacial strength at the strain rate of 10^{11} s^{-1}. We observe that all two-layered oxidized and non-oxidized films separate from the interfaces (Figure S8 in Supplementary Material), which is consistent with the MD predictions as shown in Fig. 5(c). Fig. 5(d) shows the tensile stress-strain curves of the two-layered films (∼3.1 nm in total thickness) with various oxygen atom coverages. Compared with the films without oxygen atoms, the interfacial strengths of the films increase significantly up to 1.04 O per nm^2. However, as the oxygen coverage is increased to 2.08 O per nm^2, the interface strength decreases significantly, which we ascribed to the initiation of defects in the monolayers. We think there are two competition mechanisms with increasing coverage of oxygen. One is to strengthen the interface strength due to the introduction of O atoms, which trends to improve the energy dissipation capacity during impact due to the fact that the debonding of the interfaces contributes to the dissipation of impact energy. A second mechanism is the weakening of the interface strength due to the increase in surface roughness after oxidation, as shown in Figure S9 in the Supplementary Material, which could be regarded as a kind of defect. With increasing O coverage from 0 to 1.04 per nm^2, the strengthening mechanism predominates, leading to the increase in strength. However, for the excessive O coverage of 2.08 per nm^2, the weakening mechanism facilitates premature failure of the film near the rough interface which decreases the strength, leading to the decrease of the impact resistance of the multilayered film as shown in Fig. 5(b).

4. Conclusion

In this work, we developed the layer-by-layer assembly method to fabricate multilayered Ni_2Ta MG nanofilms with excellent impact resistance. The impact resistance and the deformation behavior of multilayered MG nanofilms were obtained by laser-induced micro-ballistic impact experiments. We demonstrate that the impact resistance of multilayered oxidation MG nanofilms can be increased significantly by lamination of monolayers to

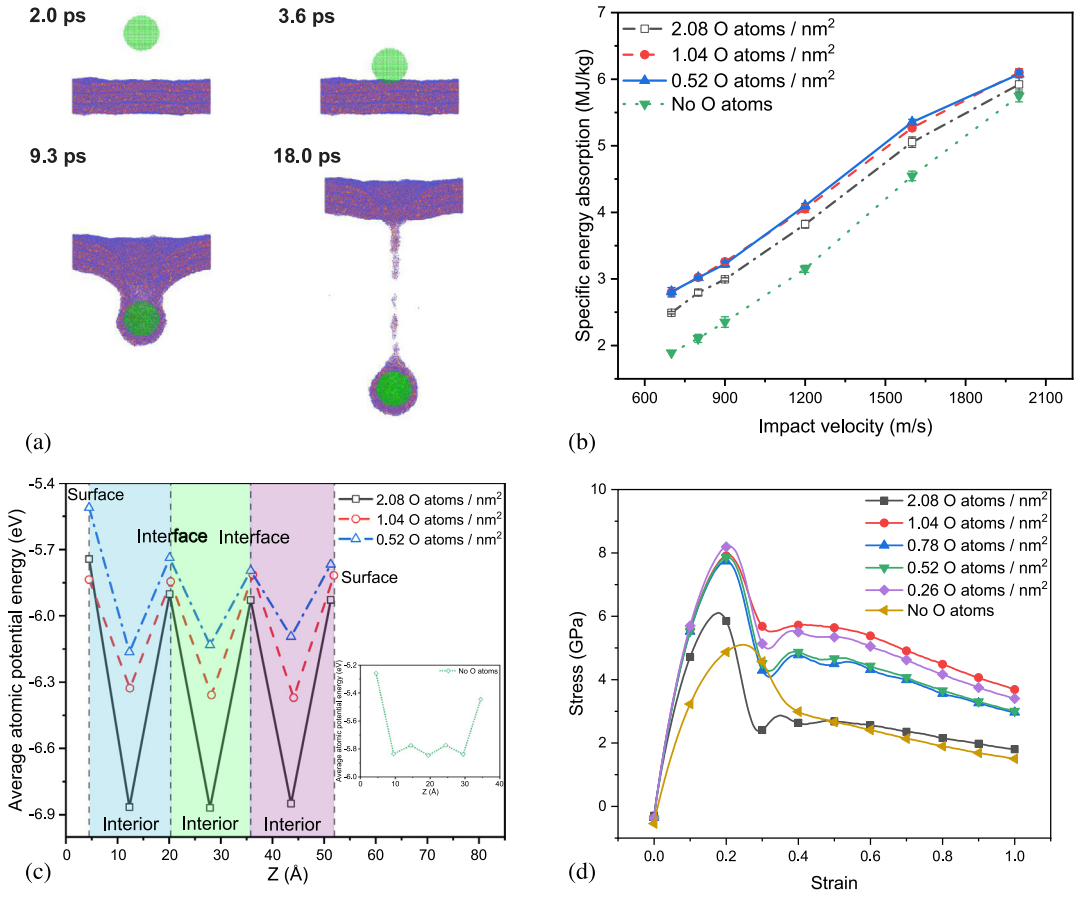

Fig. 5. (a) Deformation history of the three-layered film with a total thickness of 4.7 nm at $v_i = 900$ m/s. (b) Specific energy absorption (E_p^*) of the Ni_2Ta MG single-layer films with various oxygen coverages in O atoms per nm^2 (∼1.5-nm-thick). (c) Average atomic potential energy for Ni_2Ta MG oxidized three-layer nanofilms with different oxygen coverages. (d) Tensile stress-strain curves of two-layer films (∼3.1-nm-thick) with different oxygen coverages ($\dot{\varepsilon} = 10^{11}\ s^{-1}$).

overcome the size effects to some extent. Shear band multiplication and delamination are dominant energy dissipation mechanisms for the multilayered films under impact. In addition, MD simulations were performed to investigate the impact response of the multilayered films at a smaller scale. We described the Ni_2Ta using the EAM method and the interaction of O with Ni_2Ta using non-bond parameters derived from DFT calculations. The addition of oxygen atoms increases the interface energy, facilitating the deformation of interfacial regions. The curly structure of the thin monolayer caused by oxidation increases the penetration force and the duration of the projectile. The MD simulations predict that the impact resistance of the multilayered films increases significantly after oxidation due to the increase in interfacial strength. However, above 2.08 O per nm^2, oxygen reduces the interfacial strength due to the initiation of defects, decreasing the impact resistance of the multilayered Ni_2Ta MG films. This work provides an effective pathway for fabricating high-performance multilayered MG films with extraordinary impact resistance by overcoming the size effects through lamination of monolayers.

CRediT authorship contribution statement

Yujie Cheng: Investigation, Visualization, Writing – original draft. **Jinlei Dong:** Investigation, Validation. **Yidi Shen:** Investigation, Software. **Fucheng Li:** Investigation, Resources. **Qi An:** Software, Methodology. **Minqiang Jiang:** Data Curation, Supervision, Funding acquisition. **Yanhui Liu:** Data Curation, Supervision. **Chenguang Huang:** Data Curation, Supervision. **William A. Goddard III:** Conceptualization, Methodology, Writing – review & editing, Funding acquisition. **Xianqian Wu:** Conceptualization, Methodology, Writing – review & editing, Funding acquisition.

Declaration of competing interest

The authors declare that they have no known competing financial interests or personal relationships that could have appeared to influence the work reported in this paper.

Data availability

Data will be made available on request.

Acknowledgments

X.W. acknowledges support from the National Key R&D Program of China (2021YFA0719200) and the National Natural Science Foundation of China (12272391 and 12232020). W.A.G. acknowledges support from the Office of Naval Research, United States (N00014-22-S-B001). M.J. acknowledges support from the National Outstanding Youth Science Fund Project of National Natural Science Foundation of China (12125206).

Appendix A. Supplementary data

Supplementary material related to this article can be found online at https://doi.org/10.1016/j.eml.2023.102067.

References

[1] I.G. Crouch, Body armour – New materials, new systems, Def. Technol. 15 (2019) 241–253, http://dx.doi.org/10.1016/j.dt.2019.02.002.

[2] E. Grossman, I. Gouzman, R. Verker, Debris/micrometeoroid impacts and synergistic effects on spacecraft materials, MRS Bull. 35 (2010) 41–47, http://dx.doi.org/10.1557/mrs2010.615.

[3] J. Schroers, W.L. Johnson, Ductile bulk metallic glass, Phys. Rev. Lett. 93 (2004) 255506, http://dx.doi.org/10.1103/PhysRevLett.93.255506.

[4] T.Y. Ju, H.F. Zhou, Pressure-induced maximum shear strength and transition from shear banding to uniform plasticity in metallic glass, Extreme Mech. Lett. 41 (2020) 101058, http://dx.doi.org/10.1016/j.eml.2020.101058.

[5] W.H. Wang, Dynamic relaxations and relaxation-property relationships in metallic glasses, Prog. Mater. Sci. 106 (2019) 100561, http://dx.doi.org/10.1016/j.pmatsci.2019.03.006.

[6] X. Huang, Z. Ling, Z.D. Liu, H.S. Zhang, L.H. Dai, Amorphous alloy reinforced whipple shield structure, Internat. J. Engrg. Sci. 42 (2012) 1–10, http://dx.doi.org/10.1016/j.ijimpeng.2011.11.001.

[7] D.C. Hofmann, L. Hamill, E. Christiansen, S. Nutt, Hypervelocity impact testing of a metallic glass-stuffed whipple shield, Adv. Eng. Mater. 17 (2015) 1313–1322, http://dx.doi.org/10.1002/adem.201400518.

[8] J.L. Dong, X. Song, Z.J. Wang, K.L. Xiao, Y.H. Liu, G. Wilde, X.Q. Wu, M.Q. Jiang, Impact resistance of single-layer metallic glass nanofilms to high-velocity micro-particle penetration, Extreme Mech. Lett. 44 (2021) 101258, http://dx.doi.org/10.1016/j.eml.2021.101258.

[9] B.L. Lee, T.F. Walsh, S.T. Won, H.M. Patts, J.W. Song, A.H. Mayer, Penetration failure mechanisms of armor-grade fiber composites under impact, J. Compos. Mater. 35 (2001) 1605–1633, http://dx.doi.org/10.1106/yrbh-jgt9-u6pt-l555.

[10] Y.J. Cheng, J.L. Dong, F.C. Li, Y.D. Shen, Q. An, K.L. Xiao, M.Q. Jiang, Y.H. Liu, C.G. Huang, X.Q. Wu, Scaling law for impact resistance of amorphous alloys connecting atomistic molecular dynamics with macroscale experiments, ACS Appl. Mater. Interfaces 15 (2023) 13449–13459, http://dx.doi.org/10.1021/acsami.2c19719.

[11] J.J. Richardson, M. Bjornmalm, F. Caruso, Multilayer. assembly, Technology-driven layer-by-layer assembly of nanofilms, Science 348 (2015) aaa2491, http://dx.doi.org/10.1126/science.aaa2491.

[12] S. Sadeghzadeh, Benchmarking the penetration-resistance efficiency of multilayer graphene sheets due to spacing the graphene layers, Appl. Phys. A 122 (2016) 1–12, http://dx.doi.org/10.1007/s00339-016-0186-5.

[13] R. Zhang, B. Han, J.Y. Zhong, L.S. Qiang, C.Y. Ni, Q. Zhang, Q.C. Zhang, B.C. Li, T.J. Lu, Enhanced ballistic resistance of multilayered cross-ply UHMWPE laminated plates, Internat. J. Engrg. Sci. 159 (2022) 104035, http://dx.doi.org/10.1016/j.ijimpeng.2021.104035.

[14] M.A.N. Dewapriya, R.E. Miller, Molecular dynamics study of the penetration resistance of multilayer polymer/ceramic nanocomposites under supersonic projectile impacts, Extreme Mech. Lett. 44 (2021) 101238, http://dx.doi.org/10.1016/j.eml.2021.101238.

[15] Y.M. Wang, Q. Wang, J.J. Zhao, C. Dong, Ni–Ta binary bulk metallic glasses, Scr. Mater. 63 (2010) 178–180, http://dx.doi.org/10.1016/j.scriptamat.2010.03.044.

[16] J.H. Lee, P.E. Loya, J. Lou, E.L. Thomas, Dynamic mechanical behavior of multilayer graphene via supersonic projectile penetration, Science 346 (2014) 1092–1096, http://dx.doi.org/10.1126/science.1258544.

[17] D. Veysset, A.J. Hsieh, S. Kooi, A.A. Maznev, K.A. Masser, K.A. Nelson, Dynamics of supersonic microparticle impact on elastomers revealed by real-time multi-frame imaging, Sci. Rep. 6 (2016) 25577, http://dx.doi.org/10.1038/srep25577.

[18] M. Hassani-Gangaraj, D. Veysset, K.A. Nelson, C.A. Schuh, Melting Can Hinder impact-induced adhesion, Phys. Rev. Lett. 119 (2017) 175701, http://dx.doi.org/10.1103/PhysRevLett.119.175701.

[19] S. Plimpton, Fast parallel algorithms for short-range molecular-dynamics, J. Comput. Phys. 117 (1995) 1–19, http://dx.doi.org/10.1006/jcph.1995.1039.

[20] L.A. Zepeda-Ruiz, A. Stukowski, T. Oppelstrup, V.V. Bulatov, Probing the limits of metal plasticity with molecular dynamics simulations, Nature 550 (2017) 492–495, http://dx.doi.org/10.1038/nature23472.

[21] X.W. Zhou, R.A. Johnson, H.N.G. Wadley, Misfit-energy-increasing dislocations in vapor-deposited CoFe/NiFe multilayers, Phys. Rev. B 69 (2004) 144113, http://dx.doi.org/10.1103/PhysRevB.69.144113.

[22] F. Zhang, M.I. Mendelev, Y. Zhang, C.Z. Wang, M.J. Kramer, K.M. Ho, Effects of sub-Tg annealing on Cu64.5Zr35.5 glasses: A molecular dynamics study, Appl. Phys. Lett. 104 (2014) 061905, http://dx.doi.org/10.1063/1.4864652.

[23] G. Kresse, J. Furthmuller, Efficiency of ab-initio total energy calculations for metals and semiconductors using a plane-wave basis set, Comp. Mater. Sci. 6 (1996) 15–50, http://dx.doi.org/10.1016/0927-0256(96)00008-0.

[24] G. Kresse, J. Furthmuller, Efficient iterative schemes for ab initio total-energy calculations using a plane-wave basis set, Phys. Rev. B Condens. Matter. 54 (1996) 11169–11186, http://dx.doi.org/10.1103/physrevb.54.11169.

[25] P.M. Morse, Diatomic molecules according to the wave mechanics II. vibrational levels, Phys. Rev. 34 (1929) 57–64, http://dx.doi.org/10.1103/PhysRev.34.57.

[26] G. Kresse, J. Hafner, Ab initio molecular dynamics for liquid metals, Phys. Rev. B Condens. Matter. 47 (1993) 558–561, http://dx.doi.org/10.1103/physrevb.47.558.

[27] G. Kresse, D. Joubert, From ultrasoft pseudopotentials to the projector augmented-wave method, Phys. Rev. B 59 (1999) 1758–1775, http://dx.doi.org/10.1103/PhysRevB.59.1758.

[28] S. Grimme, S. Ehrlich, L. Goerigk, Effect of the damping function in dispersion corrected density functional theory, J. Comput. Chem. 32 (2011) 1456–1465, http://dx.doi.org/10.1002/jcc.21759.

[29] P.E. Blochl, O. Jepsen, O.K. Andersen, Improved tetrahedron method for Brillouin-zone integrations, Phys. Rev. B Condens. Matter. 49 (1994) 16223–16233, http://dx.doi.org/10.1103/physrevb.49.16223.

[30] J. Neugebauer, M. Scheffler, Adsorbate-substrate and adsorbate-adsorbate interactions of Na and K adlayers on Al(111), Phys. Rev. B Condens. Matter. 46 (1992) 16067–16080, http://dx.doi.org/10.1103/physrevb.46.16067.

[31] Y.P. Li, Z.J. Xu, S.Y. Liu, J.W. Zhang, X.N. Yang, Molecular simulation of reverse osmosis for heavy metal ions using functionalized nanoporous graphenes, Comput. Mater. Sci. 139 (2017) 65–74, http://dx.doi.org/10.1016/j.commatsci.2017.07.032.

[32] Y.L. Guan, L.S. Dai, J.L. Shao, W.D. Song, Molecular dynamics study on the nanovoid collapse and local deformation in shocked Cu50Zr50 metallic glasses, J. Non Cryst. Solids 559 (2021) 120703, http://dx.doi.org/10.1016/j.jnoncrysol.2021.120703.

[33] S. Trady, M. Mazroui, A. Hasnaoui, K. Saadouni, Molecular dynamics study of atomic-level structure in monatomic metallic glass, J. Non Cryst. Solids 443 (2016) 136–142, http://dx.doi.org/10.1016/j.jnoncrysol.2016.04.004.

[34] Z.X. Meng, S.N. Keten, Unraveling the effect of material properties and geometrical factors on ballistic penetration energy of nanoscale thin films, J. Appl. Mech. 85 (2018) 121004, http://dx.doi.org/10.1115/1.4041041.

[35] A.L. Greer, Y.Q. Cheng, E. Ma, Shear bands in metallic glasses, Mater. Sci. Eng. R Rep. 74 (2013) 71–132, http://dx.doi.org/10.1016/j.mser.2013.04.001.

[36] Y. Chen, M.Q. Jiang, L.H. Dai, Collective evolution dynamics of multiple shear bands in bulk metallic glasses, Int. J. Plast. 50 (2013) 18–36, http://dx.doi.org/10.1016/j.ijplas.2013.03.010.

[37] M.A.N. Dewapriya, R.E. Miller, Energy absorption mechanisms of nanoscopic multilayer structures under ballistic impact loading, Comp. Mater. Sci. 195 (2021) http://dx.doi.org/10.1016/j.commatsci.2021.110504.